Cytoplasmic Na^+-dependent modulation of mitochondrial Ca^{2+} via electrogenic mitochondrial Na^+–Ca^{2+} exchange

Bongju Kim and Satoshi Matsuoka

Department of Physiology and Biophysics, Graduate School of Medicine, Kyoto University, Kyoto 606-8501, Japan

To clarify the role of mitochondrial Na^+–Ca^{2+} exchange (NCX_{mito}) in regulating mitochondrial Ca^{2+} (Ca^{2+}_{mito}) concentration at intact and depolarized mitochondrial membrane potential ($\Delta\Psi_{mito}$), we measured Ca^{2+}_{mito} and $\Delta\Psi_{mito}$ using fluorescence probes Rhod-2 and TMRE, respectively, in the permeabilized rat ventricular cells. Applying 300 nM cytoplasmic Ca^{2+} (Ca^{2+}_c) increased Ca^{2+}_{mito} and this increase was attenuated by cytoplasmic Na^+ (Na^+_c) with an IC_{50} of 2.4 mM. To the contrary, when $\Delta\Psi_{mito}$ was depolarized by FCCP, a mitochondrial uncoupler, Na^+_c enhanced the Ca^{2+}_c-induced increase in Ca^{2+}_{mito} with an EC_{50} of about 4 mM. This increase was not significantly affected by ruthenium red or cyclosporin A. The inhibition of NCX_{mito} by CGP-37157 further increased Ca^{2+}_{mito} when $\Delta\Psi_{mito}$ was intact, while it suppressed the Ca^{2+}_{mito} increase when $\Delta\Psi_{mito}$ was depolarized, suggesting that $\Delta\Psi_{mito}$ depolarization changed the exchange mode from forward to reverse. Furthermore, $\Delta\Psi_{mito}$ depolarization significantly reduced the Ca^{2+}_{mito} decrease via forward mode, and augmented the Ca^{2+}_{mito} increase via reverse mode. When the respiratory chain was attenuated, the induction of the reverse mode of NCX_{mito} hyperpolarized $\Delta\Psi_{mito}$, while $\Delta\Psi_{mito}$ depolarized upon inducing the forward mode of NCX_{mito}. Both changes in $\Delta\Psi_{mito}$ were remarkably inhibited by CGP-37157. The above experimental data indicated that NCX_{mito} is voltage dependent and electrogenic. This notion was supported theoretically by computer simulation studies with an NCX_{mito} model constructed based on present and previous studies, presuming a consecutive and electrogenic Na^+–Ca^{2+} exchange and a depolarization-induced increase in Na^+ flux. It is concluded that Ca^{2+}_{mito} concentration is dynamically modulated by Na^+_c and $\Delta\Psi_{mito}$ via electrogenic NCX_{mito}.

(Resubmitted 22 November 2007; accepted after revision 23 January 2008; first published online 24 January 2008)
Corresponding author S. Matsuoka: Department of Physiology and Biophysics, Graduate School of Medicine, Kyoto University, Yoshida-Konoe-cho, Sakyo-ku, Kyoto 606–8501, Japan. Email: matsuoka@card.med.kyoto-u.ac.jp

Mitochondria in the cardiac myocyte have been recognized as Ca^{2+} stores, in addition to their role as energy providers that synthesise a large proportion of ATP required for maintaining heart function. Mitochondrial Ca^{2+} (Ca^{2+}_{mito}) activates matrix dehydrogenases (pyruvate dehydrogenase, isocitrate dehydrogenase and α-ketoglutarate dehydrogenase) (McCormack *et al.* 1990) and may also activate F_0/F_1-ATPase (Territo *et al.* 2000). The overall effect of elevated Ca^{2+}_{mito} may be the up-regulation of oxidative phosphorylation and the acceleration of ATP synthesis (McCormack *et al.* 1990; Balaban, 2002; Matsuoka *et al.* 2004; Jo *et al.* 2006). On the other hand, the excessive rise in Ca^{2+}_{mito} triggers the mitochondrial permeability transition pore (PTP) resulting in pathological cell injury and death (Weiss *et al.* 2003; Brookes *et al.* 2004; Hajnoczky *et al.* 2006). Therefore, the Ca^{2+}_{mito} concentration must be kept within the proper range to maintain physiological mitochondrial function.

In cardiac mitochondria, Ca^{2+} uptake and removal is mainly mediated via the mitochondrial Ca^{2+} uniporter and the Na^+–Ca^{2+} exchange (NCX_{mito}) (Gunter & Pfeiffer, 1990; Bernardi, 1999; Brookes *et al.* 2004), respectively. The mitochondria Ca^{2+} uniporter is driven by the mitochondrial membrane potential ($\Delta\Psi_{mito}$) (Rottenberg & Scarpa, 1974; O'Rourke, 2007) and a recent patch clamp study demonstrated that it is an ion channel highly selective to Ca^{2+} (Kirichok *et al.* 2004). On the other hand, the dependence of NCX_{mito} on $\Delta\Psi_{mito}$ has been controversial and an electrophysiological approach for measuring current mediated via NCX_{mito} has not succeeded.

NCX_{mito} was first discovered by Carafoli *et al.* (1974). Electrogenic or voltage-dependent Na^+–Ca^{2+} exchange was suggested by their later studies demonstrating the higher Hill coefficient (n_H) for Na^+_c ($\sim$3) and the attenuation of Na^+-dependent Ca^{2+} efflux by $\Delta\Psi_{mito}$ depolarization induced by an uncoupler (Crompton

 DOI: 10.1113/jphysiol.2007.148726

et al. 1976, 1977). A later study by Jung *et al.* (1995) further supported this notion by measuring matrix pH and Ca^{2+} with fluorescence probes. To the contrary, Affolter & Carafoli (1980) demonstrated that $\Delta\Psi_{mito}$ did not alter when the Ca^{2+} efflux via NCX_{mito} was induced and suggested NCX_{mito} is electroneutral. Brand (1985) also suggested the voltage-independent exchange by demonstrating that Ca^{2+} efflux via NCX_{mito} was not affected by A23187, which catalyses Ca^{2+}–$2H^+$ exchange. Wingrove & Gunter (1986) supported this idea by in-depth measurements of the Na_c^+ and Ca_c^{2+} dependences ($n_H = 2.0$ and 1.0, respectively). Therefore, it is a prerequisite to clarify whether NCX_{mito} depends on $\Delta\Psi_{mito}$ in order to quantitatively understand the mechanisms regulating Ca_{mito}^{2+} concentration.

$\Delta\Psi_{mito}$ depolarizes under various pathological conditions such as ischaemia/reperfusion (see reviews, for example, Weiss *et al.* 2003). Under such circumstance, cytoplasmic Na^+ (Na_c^+) as well as Ca^{2+} (Ca_c^{2+}) concentrations increase (Pierce & Czubryt, 1995; Piper *et al.* 2003). While the increase in Ca_c^{2+} concentration leads to the accumulation of Ca^{2+} in mitochondria, only limited information is available about how Na_c^+ affects Ca_{mito}^{2+} concentration and NCX_{mito} activity when $\Delta\Psi_{mito}$ is depolarized (Smets *et al.* 2004; Saotome *et al.* 2005). Saotome *et al.* (2005) recently reported a slight decrease in the affinity for Na_c^+ of the Ca^{2+} efflux via NCX_{mito} when $\Delta\Psi_{mito}$ was dissipated, which is in contrast to the larger effect found by Crompton *et al.* (1977).

In the present study, we aimed to clarify how the changes in Na_c^+ concentration and $\Delta\Psi_{mito}$ modulate the Ca_{mito}^{2+} concentration of cardiac mitochondria, and how NCX_{mito} is involved in the modulation. Our experimental and simulation studies indicated that NCX_{mito} is voltage dependent and electrogenic. Because of this feature, NCX_{mito} dynamically changes the exchange mode (forward or reverse) and modulates the Ca_{mito}^{2+} concentration in a manner dependent on Na_c^+ and $\Delta\Psi_{mito}$.

Methods

Cell isolation

Ventricular myocytes were obtained from male Wister rats (body wt, 250–350 g) in a similar manner to recent articles (Lin *et al.* 2006; Shioya, 2007). This protocol was approved by the Animal Research Committee in the Graduate School of Medicine, Kyoto University. In brief, Wister rats were anaesthetized by intraperitoneal administration of pentobarbitone sodium ($> 0.1\ mg\ g^{-1}$). The heart was quickly excised after thoracotomy and mounted on a Langendorff apparatus to perfuse through the coronary artery with a Ca^{2+}-free cell isolation buffer (CIB) at 37°C. After 8–10 min perfusion to clear the blood and to stop the heart beating, the CIB solution containing 0.2 mM Ca^{2+}, collagenase (Type II, $1\ mg\ ml^{-1}$ Worthington), protease (Type XIV, $0.05\ mg\ ml^{-1}$ Sigma-Aldrich) and trypsin (Type I, $0.05\ mg\ ml^{-1}$ Sigma-Aldrich) was perfused for 10–15 min. The left ventricle was then cut into small pieces and was shaken gently for 5–10 min in the CIB solution, to which 0.3 mM Ca^{2+} and $1\ mg\ ml^{-1}$ bovine serum albumin (Sigma-Aldrich) were added. Finally, isolated myocytes were transferred to the CIB solution containing 1 mM Ca^{2+} and then stored in a modified DMEM solution.

Solutions and drugs

The CIB solutions contained (mM): 130 NaCl, 5.4 KCl, 0.5 $MgCl_2$, 0.33 NaH_2PO_4, 22 glucose, 1 L-gutamine, 0.1 EGTA, 25 Hepes, and 0.01 units ml^{-1} insulin (pH 7.4 with NaOH). The modified DMEM solution was prepared by adding 20 mM NaCl, 25 mM Hepes to DMEM (without $NaHCO_3$, MP Biomedicals) (pH 7.4 with NaOH). The bath solution contained (mM): 118 KCl, 10 EGTA, 10 Hepes, 3 K_2ATP, 2 potassium pyruvate, 1 K_2HPO_4, 2 succinic acid, 0.1 K-ADP, 2 malic acid, and 2 potassium glutamic acid (pH 7.2 with KOH). Free Mg^{2+} and Ca^{2+} concentrations, which were calculated by WinMAXC software (Patton *et al.* 2004), were adjusted to be 1 mM and 300–800 nM, respectively, by adding 4.02–4.99 mM $MgCl_2$ and 6.65–8.41 mM $CaCl_2$. Na_c^+ concentration was changed from 0 to 50 mM by replacing KCl with equimolar NaCl.

Ruthenium red (an inhibitor of the mitochondrial Ca^{2+} uniportor), cyclosporin A (an inhibitor of PTP), antimycin A (an inhibitor of complex III of the mitochondrial electron transport chain), oligomycin (an inhibitor of F_0/F_1-ATPase), NS1619 (an opener of mitochondrial Ca^{2+}-activated K^+ channel), and carbonyl cyanide 4-(trifluoromethoxy) phenylhydrazone (FCCP, an ionopore of protons) were purchased from Sigma-Aldrich, and CGP-37157 (an inhibitor of NCX_{mito}) was from Tocris Cookson Inc. SM20550 (an inhibitor of mitochondrial Na^+–H^+ exchange) was a kind gift from Dainippon Sumitomo Phama. CGP-37157 (20 mM), cyclosporin A (1 mM), antimycin A (10 mM), oligomycin (10 mM), FCCP (1 mM) and NS1619 (10 mM) were dissolved in DMSO as stock solutions. The final concentration of DMSO in the bath solution was 0.01–0.1%. Cyclosporin A (0.1 μM) was added to the bath solution when $\Delta\Psi_{mito}$ was depolarized or mitochondria were preloaded with a high Ca_c^{2+} (600 or 800 nM) unless otherwise stated. 2,3-butaedione monoxine (20 mM; BDM; Sigma-Aldrich) was added to the bath solution to reduce contraction artifacts when applying a high Ca_c^{2+} concentration (600 or 800 nM).

The bath solution was changed within 2–3 s by using a perfusion system (ValveLink8, AutoMate Scientifi Inc., USA).

Measurement of Ca^{2+}_{mito} and $\Delta\Psi_{mito}$ in permeabilized myocytes

The myocytes were loaded with TMRE (an indicator for the mitochondrial membrane potential; Molecular Probes, Eugene, OR, USA), a permeant AM-ester form of Rhod-2 (a cationic indicator for Ca^{2+}; Molecular Probes), or MitoTracker Green (a mitochondria-specific dye; Molecular Probes). To remove the fluorescence dyes from cytoplasm and to facilitate access to mitochondria, sarcolemmal membrane was permeabilized by applying a Ca^{2+}-free bath solution containing saponin (0.1 mg ml^{-1}) for 1 min, according to previous studies (Fry *et al.* 1984; Sedova & Blatter, 2000; Saotome *et al.* 2005). Fluorescence images were obtained at 36–37°C by using a laser scanning confocal microscope (FV500 Olympus, Japan) with a ×40 water-immersion objective lens. All the images were recorded by a single scan every 10 or 20 s, except for those in Fig. 1 (an average of five consecutive scans). Myocytes loaded with TMRE or Rhod-2 were excited at 543 nm, and the fluorescence images at > 560 nM (TMRE) or 560–600 nM (Rhod-2) were obtained. When co-loaded with MitoTracker Green (excitation; 488 nM) and Rhod-2 (excitation: 543 nm), fluorescence images at 505–525 nM and 560–600 nM, respectively, were sequentially obtained.

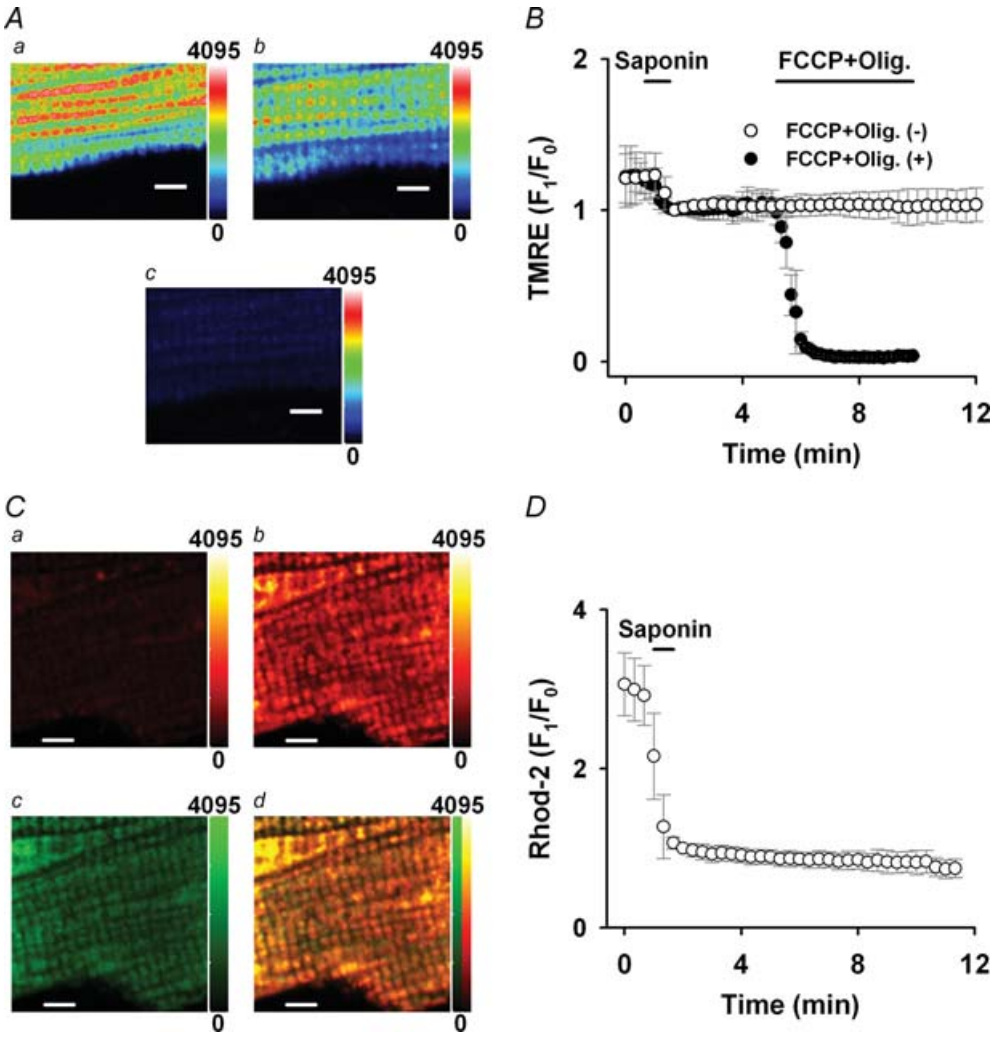

Figure 1. Measurement of Ca^{2+}_{mito} and $\Delta\Psi_{mito}$
A, confocal images of a myocyte loaded with TMRE before (*a*) and after (*b*) saponin treatment, and 4 min after applying 1 μM FCCP and 2 μM oligomycin (*c*). *B*, time course of TMRE fluorescence change with (●) or without (○) applying 1 μM FCCP and 2 μM oligomycin (FCCP + Olig). *C*, confocal images of a myocyte co-loaded with Rhod-2 and MitoTracker Green after saponin treatment. Rhod-2 images before (*a*) and 5 min after (*b*) applying 600 nM Ca^{2+}, MitoTracker Green image 5 min after applying 600 nM Ca^{2+} (*c*), and a merged image of Rhod-2 and MitoTracker Green image (*d*). *D*, time course of Rhod-2 fluorescence change. In *A* and *C*, the colour scale of fluorescence intensity is denoted on the right side (arbitrary units) and a bar indicates 5 μm in each image. In *B* and *D*, the TMRE and Rhod-2 fluorescences were normalized to the first one after the saponin treatment.

The fluorescence intensity (F) of TMRE or Rhod-2 within the cell area was obtained by subtracting a background component as follows:

$$F = F_{\text{cell}} - F_{\text{background}}$$

where F_{cell} and $F_{\text{background}}$ are an average of fluorescence from the entire cell area and the extracellular area, respectively.

For the measurement of $\Delta\Psi_{\text{mito}}$, the myocytes were loaded with 25 nM TMRE for 10 min at room temperature. To reduce TMRE fluorescence loss, 12.5 nM TMRE was added to the bath solution. Figure 1*A* demonstrates TMRE fluorescence images before (a) and after (b) the saponin treatment (0 Ca^{2+}). The fluorescence pattern was similar to that of MitoTracker Green in Fig. 1*Cc* and fluorescence in the extracellular area was almost negligible (3–4% of cellular area). The saponin treatment decreased the TMRE fluorescence about by 20%, but did not affect the mitochondrial alignment. Most of the remaining fluorescence reflects $\Delta\Psi_{\text{mito}}$, whose value is about −150 to −180 mV under the normal condition (Nicholls & Budd, 2000). Applying 1 μM FCCP and 2 μM oligomycin abolished the TMRE fluorescence (Fig. 1*Ac*; 3 min after), indicating depolarization of $\Delta\Psi_{\text{mito}}$. The TMRE fluorescence was stable over 10 min as shown in Fig. 1*B* (open circles). In the present study, $\Delta\Psi_{\text{mito}}$ was depolarized with a variety of procedures illustrated by an example in Fig. 1*B* (filled circles; 1 μM FCCP and 2 μM oligomycin (FCCP + Olig.)) and change of $\Delta\Psi_{\text{mito}}$ (mV) was estimated according to a study by O'Reilly *et al.* (2003) as follows:

$$61.5 \times \log(F_0/F_1),$$

where F_0 and F_1 are an average fluorescence intensity of TMRE in the cell area, from which the background fluorescence was subtracted, before and after the procedures, respectively. Table 1 summarizes the change of $\Delta\Psi_{\text{mito}}$ and the half-time to steady state ($t_{1/2}$).

For the measurement of Ca^{2+}_{mito}, rat myocytes were loaded with 5 μM Rhod-2 for 60 min at 4°C as described in previous studies (Trolinger *et al.* 1997; Jo *et al.* 2006). Rhod-2 was located also in the cytoplasm after the loading (data not shown), but the saponin treatment greatly washed it out (Fig. 1*Ca*). Localization of Rhod-2 in mitochondria was confirmed in the myocytes by further loading of 200 nM MitoTracker Green for 30 min at 37°C. The Rhod-2 fluorescent was slightly visible after the saponin treatment (Fig. 1*Ca*; 0 nM Ca^{2+}), while the fluorescence from unloaded control myocytes was not detectable (not shown). Applying Ca^{2+} remarkably but locally increased the fluorescence intensity (Fig. 1*Cb*; 5 min after applying 600 nM Ca^{2+}). Figure 1*Cc* is an image of MitoTracker Green from the same cell and a merged image of panel *b* and *c* is shown in panel *d*, indicating that fluorescences of Rhod-2 and MitoTracker Green were largely co-localized. On average, 96 ± 3% ($n = 5$) of the MitoTracker Green fluorescence co-localized with the Rhod-2 fluorescence. Therefore we concluded that the Rhod-2 almost exclusively monitors Ca^{2+} in mitochondria under the present experimental conditions. The Rhod-2 fluorescence was stable over 10 min and did not show significant photo bleaching as shown in Fig. 1*D*.

Table 1. Summary of $\Delta\Psi_{\text{mito}}$ change

	Estimated change in $\Delta\Psi_{\text{mito}}$ (mV)	$t_{1/2}$ (s)
Sub(−)	78 ± 25	132 ± 34 ($n = 6$)
FCCP	104 ± 4	30 ± 4 ($n = 10$)
FCCP + Olig	101 ± 4	36 ± 10 ($n = 7$)
Anti + Olig	104 ± 3	87 ± 26 ($n = 7$)
NS1619	75 ± 21	282 ± 91 ($n = 7$)
NS1619 + Sub(−)	97 ± 11	154 ± 47 ($n = 10$)

Sub(−); removal of mitochondrial substrates (potassium pyruvate, K_2HPO_4, succinic acid, K-ADP, malic acid, and potassium glutamic acid); FCCP; 1 μM FCCP; FCCP + Olig; 1 μM FCCP and 2 μM oligomycin; Anti + Olig; 10 μM antimycin A and 2 μM oligomycin; NS1619; 10 μM NS1619; and NS1619 + Sub(−); 10 μM NS1619 without the mitochondrial substrates.

Statistical analysis

Data are presented as mean ± S.D. Statistical analyses were performed by one-factor ANOVA using StatView (SAS Institute Inc.). Multiple and two-group comparisons were performed according to Student–Newman–Keul's method and Student's t test, respectively. $P < 0.05$ was considered significant.

A computer model of NCX_{mito}

A computer model of NCX_{mito} was constructed using Visual Studio 2005 (Microsoft). Details are described in the Appendix.

Results

Na^+_c dependence of Ca^{2+}_{mito}

Dependence of Ca^{2+}_{mito} concentration on Na^+_c was first examined at intact $\Delta\Psi_{\text{mito}}$ in Fig. 2. An increase in Ca^{2+}_c from 0 to 300 nM greatly augmented Ca^{2+}_{mito}, which was measured by Rhod-2, in the absence of Na^+_c (white circles). The rise was 9.2 ± 2.8 times on average and it took about 10 min to reach steady state. The rise of Rhod-2 fluorescence was almost completely inhibited by 7 μM ruthenium red (grey triangles), an inhibitor of the mitochondrial Ca^{2+} uniporter ($IC_{50} = 9$ nM; Kirichok *et al.* 2004), supporting the previous notion that the Ca^{2+}

uniporter is the dominant mechanism of Ca^{2+}_{mito} influx (Gunter & Pfeiffer, 1990; Bernardi, 1999). The maximum Ca^{2+}_{mito} level decreased with increasing Na^+_c concentration. Averages of the maximum increase were 5.5, 3.4, 2.3 and 1.4 times in the presence of 2, 6, 20 and 50 mM Na^+_c, respectively. The Na^+_c-dependent decrease is most probably due to Ca^{2+}_{mito} removal via NCX_{mito}. Fitting a Hill equation to the maximum Rhod-2 fluorescence levels yielded a half-inhibitory concentration (IC_{50}) of 2.4 mM Na^+ (Fig. 2*B*).

On the other hand, an opposite Na^+_c dependence was obtained when $\Delta\Psi_{mito}$ was depolarized. In Fig. 2*C*, the myocytes were first superfused with the bath solution containing 1 μM FCCP, which greatly depolarized $\Delta\Psi_{mito}$ (see Table 1). Applying 300 nM Ca^{2+} increased the Rhod-2 fluorescence only 1.7 times in the absence of Na^+_c. However, with 6 or 20 mM Na^+_c, the rise was augmented to 2.5 and 3.1 times, respectively. A further increase of Na^+_c to 50 mM attenuated the fluorescence intensity. The half-effective concentration (EC_{50}) for Na^+_c was about 4 mM (Fig. 2*D*). Under this experimental condition, the Ca^{2+}_c-induced Ca^{2+}_{mito} increase might be due to mechanism(s) different from the Ca^{2+} uniporter because the Ca^{2+} influx through the channel was likely to be largely attenuated when $\Delta\Psi_{mito}$ is depolarized (Rottenberg & Scarpa, 1974; O'Rourke, 2007). Consistent with this notion, ruthenium

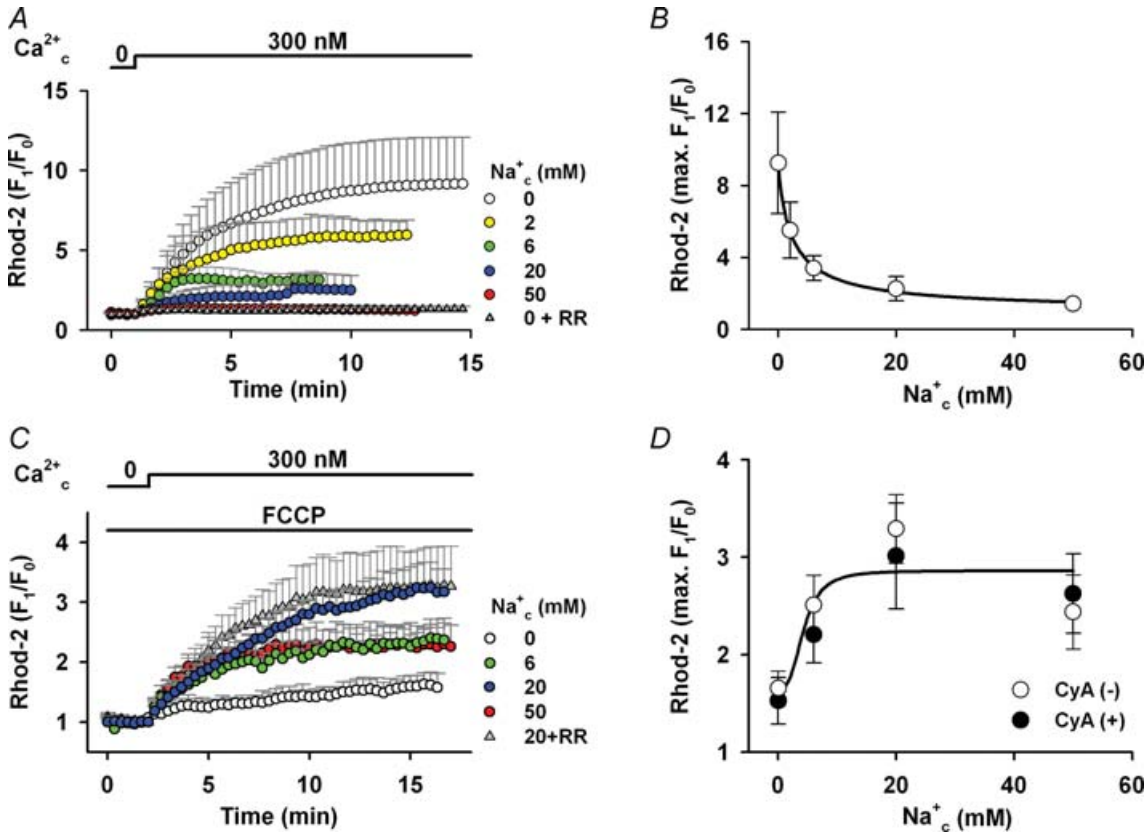

Figure 2. Effects of Na^+_c on Ca^{2+}_{mito}
A, Ca^{2+}_c-induced Ca^{2+}_{mito} increase at intact $\Delta\Psi_{mito}$. Ca^{2+}_c (300 nM) was added in the presence of various concentrations of Na^+_c as denoted at the top and right of graph. Ruthenium red (RR; 7 μM) was added to the Na^+-free solution (grey triangles, $n = 10$). The Rhod-2 fluorescence was normalized to the one before applying Ca^{2+}_c. *B*, Na^+_c dependence of Ca^{2+}_{mito}. The maximum increases of Rhod-2 fluoresce in *A* (9.2 ± 2.8, 5.5 ± 1.6, 3.4 ± 0.7, 2.3 ± 0.7 and 1.4 ± 0.2 times, in the presence of 0, 2, 6, 20 and 50 mM Na^+_c, respectively) were plotted against Na^+_c concentration. The curve is a fitted equation: $1.0 + 8.2/(1 + (Na^+_c/2.4)^{0.9})$. $n = 4$–23. *C*, Ca^{2+}_c-induced Ca^{2+}_{mito} increase at depolarized $\Delta\Psi_{mito}$. The same protocol as in *A* was repeated in the presence of 1 μM FCCP. RR (7 μM) was added to the solution containing 20 mM Na^+ (grey triangles, $n = 9$). *D*, the maximum increases of Rhod-2 fluoresce (○) in *C* (1.7 ± 0.2, 2.5 ± 0.3, 3.3 ± 0.4 and 2.4 ± 0.4 times in the presence of 0, 6, 20 and 50 mM Na^+_c, respectively) were plotted. The curve is a fitted equation: $1.7 + 1.2/(1 + (4.3/Na^+_c)^{3.0})$. $n = 5$–11. Data with cyclosporin A (●) are 1.5 ± 0.2, 2.2 ± 0.3, 3.0 ± 0.5 and 2.6 ± 0.4 times in the presence of 0, 6, 20 and 50 mM Na^+_c, respectively. $n = 4$–7. The maximum increases were not significantly different in the absence and presence of the drug at each Na^+_c concentration.

red did not significantly affect the Ca^{2+}_{mito} increase (Fig. 2*C*; grey triangles; 20 mM Na^+_c + 7 μM ruthenium red). The involvement of PTP in the Ca^{2+}_c-induced Ca^{2+}_{mito} increase is probably small because addition of 0.1 μM cyclosporin A, which is a potent inhibitor of PTP (IC_{50} = 25 nM; McGuinness *et al.* 1990), to the bath solution did not greatly affect the Ca^{2+}_{mito} increase (filled circles in Fig. 2*D*).

One of the major Ca^{2+} handling mechanisms of cardiac mitochondria is NCX_{mito}, which exchanges Ca^{2+}_{mito} for Na^+_c (Crompton *et al.* 1976, 1977; Bernardi, 1999). We hypothesized that NCX_{mito} is involved in the Ca^{2+}_c-induced Ca^{2+}_{mito} increase at both intact and depolarized $\Delta\Psi_{mito}$. This hypothesis was first tested pharmacologically in Fig. 3. As we expected, applying 30 μM CGP-37157, which almost completely suppresses NCX_{mito} (IC_{50} = 0.36 μM; Cox *et al.* 1993; also see Fig. 4*A*), after the application of 300 nM Ca^{2+}_c and 6 mM Na^+_c induced a further increase in the Rhod-2 fluorescence when $\Delta\Psi_{mito}$ was intact (Fig. 3*A*). This result indicates that the forward mode of NCX_{mito} operates under this condition, attenuating Ca^{2+}_{mito} increase due to Ca^{2+} influx through the Ca^{2+} uniporter. To the contrary, when $\Delta\Psi_{mito}$ was depolarized by 1 μM FCCP (Fig. 3*B*), CGP-37157 attenuated the increase in Rhod-2 fluorescence (3.4 *versus* 1.4 times, $P < 0.05$) and a removal of the drug induced a fluorescence increase. This result suggested that the Ca^{2+}_{mito} increase was mediated by the Ca^{2+} influx through the reverse mode of NCX_{mito}, not via the Ca^{2+} uniporter. Therefore, it was suggested that NCX_{mito} mediates the Na^+_c-dependent Ca^{2+}_{mito} extrusion (forward mode of exchange) when $\Delta\Psi_{mito}$ is intact, while the exchange mode reverses when $\Delta\Psi_{mito}$ depolarizes. Dependences of NCX_{mito} on Na^+_c and $\Delta\Psi_{mito}$ were studied in detail in the following experiments.

Ca^{2+} efflux through the forward mode of NCX_{mito}

In Fig. 4, the Na^+_c dependence of the forward mode of NCX_{mito} was studied under the condition where NCX_{mito} mainly operates Ca^{2+} efflux from mitochondria. The myocytes were first preloaded with Ca^{2+} by superfusing with bath solution containing 300 nM Ca^{2+}_c and no Na^+_c until the Rhod-2 fluorescence reached a steady state. Switching the bath solution to one containing no Ca^{2+}_c and 6 mM Na^+_c induced a decay of Rhod-2 fluorescence with a half-time to steady state ($t_{1/2}$) of about 60 s (open circles). With 30 μM CGP-37157 (filled circles) or no Na^+ (open triangles), the decay was significantly attenuated and did not reach a steady state within 30 min. The initial decay velocity (% min^{-1}) was plotted against Na^+_c concentration (Fig. 4*B*). The half-maximum concentration ($K_{1/2}$) of Na^+_c was about 1 mM, a value which is comparable to the IC_{50} in Fig. 2*B*. The high Hill coefficient (n_H = 3.8) suggests that more than three Na^+ are transported.

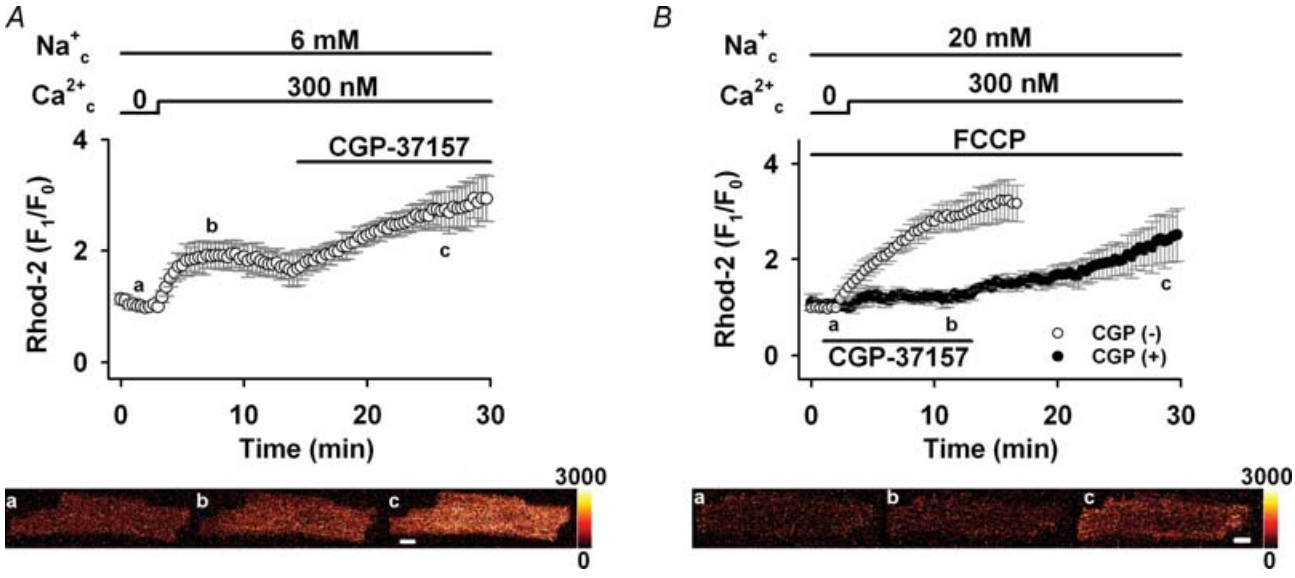

Figure 3. Effects of NCX_{mito} inhibition on Ca^{2+}_c-induced Ca^{2+}_{mito} increase
A, inhibition of forward mode of NCX_{mito} at normal $\Delta\Psi_{mito}$. After reaching a steady state of Rhod-2 fluorescence, 30 μM CGP-37157 was added to the bath solution. n = 6. Representative images of a myocyte loaded with Rhod-2 before (*a*) and after (*b*) adding Ca^{2+}_c, and 15 min after applying CGP-37157 (*c*) are shown in the lower panel. *B*, inhibition of reverse mode of NCX_{mito} at depolarized $\Delta\Psi_{mito}$. The protocol is the same as in Fig. 2*C* and 30 μM CGP-37157 was added prior to the application of 300 nM Ca^{2+}_c (●, n = 5). The maximum increase with and without CGP-37157 was significantly different. Representative images are shown in the lower panel. The colour scale of fluorescence intensity is denoted on the right side (arbitrary units) and a bar indicates 10 μm.

The voltage dependence of NCX_{mito} has been controversial. To directly address this issue, we measured $\Delta\Psi_{mito}$ in TMRE-loaded myocytes. When the Ca^{2+} efflux via NCX_{mito} was induced with the same protocol as in Fig. 4 (6 mM Na^+_c), no significant change in the TMRE fluoresence was observed (data not shown). This result is consistent with experiments by Affolter & Carafoli (1980), but inconsistent with the $\Delta\Psi_{mito}$ dependence suggested in Figs 2 and 3. Since $\Delta\Psi_{mito}$ is largely maintained by H^+ pumping via the respiratory chain (Nicholls & Budd, 2000), NCX_{mito}-induced membrane potential change might be compensated by the respiratory chain. As expected, a large decline of the TMRE fluorescence (depolarization) was induced upon the activation of Ca^{2+} efflux via NCX_{mito} (open circles, Fig. 4*A*) when the respiratory chain was suppressed by removing mitochondria substrates (potassium pyruvate, K_2HPO_4, succinic acid, K-ADP, malic acid and potassium glutamic acid). The decline of TMRE fluorescence was largely attenuated by CGP-37157 (closed circles, Fig. 5*A*) and was significantly suppressed without mitochondria pre-loading with Ca^{2+} (triangles, Fig. 5*A*). These data demonstrated that the Ca^{2+} efflux via the forward mode of NCX_{mito} depolarizes $\Delta\Psi_{mito}$. The direction of $\Delta\Psi_{mito}$ change is consistent with that expected in plasma membrane NCX, in which positive charge is supposed to move concurrently with Na^+ flux (Hilgemann *et al.* 1991; Matsuoka & Hilgemann, 1992; Powell *et al.* 1993). The above results indicated that NCX_{mito} is electrogenic.

The $\Delta\Psi_{mito}$ dependence of Ca^{2+} efflux via NCX_{mito} was studied in Fig. 5*B*. $\Delta\Psi_{mito}$ was altered by several procedures: 1 μM FCCP (an ionopore of proton), 10 μM antimycin A (an inhibitor of complex III of the mitochondrial electron transport chain, $IC_{50} = 13$ nM; Cherednichenko *et al.* 2004) and 2 μM oligomycin (an inhibitor of F_0/F_1-ATPase, $IC_{50} \approx 0.3$ μM; Van Dyke *et al.* 1984) (Anti + Olig.), 10 μM NS1619 (an opener of mitochondrial Ca^{2+}-activated K^+ channel; Sato *et al.* 2005), and 10 μM NS1619 without mitochondrial substrates (NS1619 + Sub(−)). It was estimated that these procedures depolarized the mitochondrial membrane by approximately 104, 104, 75 and 97 mV on average, respectively (see Table 1). In Fig. 5*B*, Rhod-2-loaded myocytes were first pre-loaded with 300 nM Ca^{2+}_c until reaching a steady state; these conditions were maintained for 5–12 min to allow $\Delta\Psi_{mito}$ to reach a new steady state. Then the Ca^{2+} efflux was induced in a manner similar to Fig. 4*A* (6 mM Na^+). However, the initial decay velocity of Rhod-2 fluorescence was not significantly different between intact and depolarized mitochondria. Our computer model predicted, as shown later in Fig. 7, that the Ca^{2+} efflux via NCX_{mito} is more steeply dependent on $\Delta\Psi_{mito}$ at higher Ca^{2+}_{mito}. In line with this prediction, the initial decay velocity was largely slowed by the $\Delta\Psi_{mito}$ depolarization (FCCP, Anti + Oligo) when mitochondria was pre-loaded with 800 nM Ca^{2+} (Fig. 5*C*). The contribution of PTP and Ca^{2+} uniporter to the Rhod-2 fluorescence decay was unlikely, because

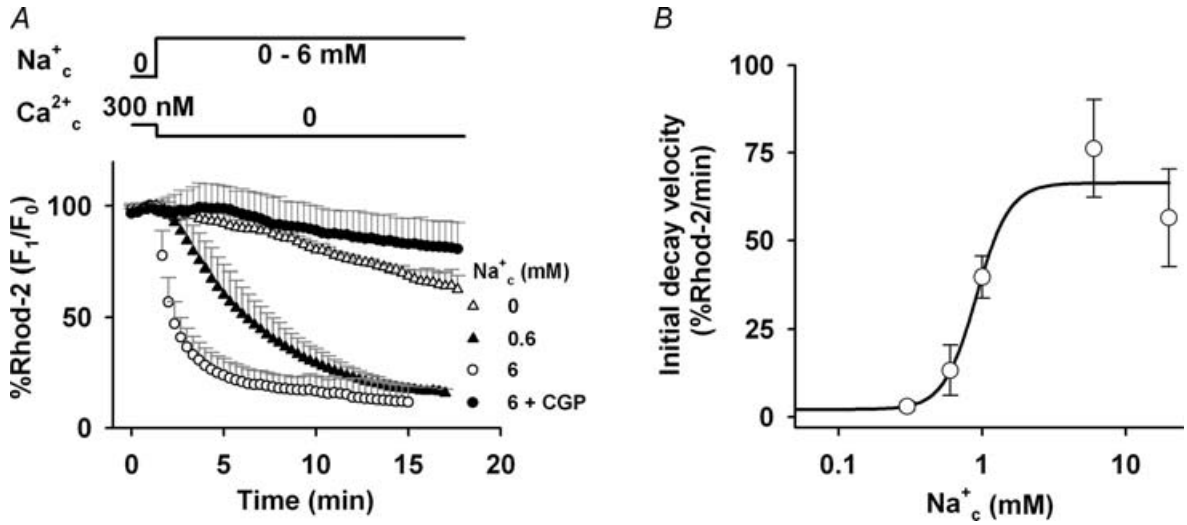

Figure 4. Na^+_c dependence of Ca^{2+} efflux via forward mode of NCX_{mito}
A, time course of Ca^{2+}_{mito} decrease. The myocytes were preloaded with 300 nM Ca^{2+}_c and Ca^{2+} efflux via forward mode of NCX_{mito} was induced by applying the bath solution with no Ca^{2+} and various Na^+_c as denoted on the right of graph. CGP-37157 (30 μM) was added to the solution with 6 mM Na^+ (●). The Rhod-2 fluorescence was normalized to that before changing the solution. *B*, Na^+_c dependence of initial decay velocity of Ca^{2+} efflux. The initial decay velocity of Ca^{2+} efflux (2.1 ± 0.4, 3.1 ± 1.3, 13.3 ± 7.1, 39.7 ± 5.9, 76.2 ± 13.9 and 56.5 ± 13.9% min^{-1} in the presence of 0, 0.3, 0.6, 1, 6 and 20 mM Na^+_c, respectively) was fitted by a Hill equation: $2.2 + 64.2/(1 + (0.9/Na^+_c)^{3.8})$. $n = 4$–7.

no significant difference was found in the initial decay velocity at intact $\Delta\Psi_{mito}$ with or without ruthenium red, which was added after the pre-loading (71.2 ± 9.6 *versus* $76.7 \pm 13.9\%\ min^{-1}$) and cyclosporin A ($78.9 \pm 18.0$ *versus* $76.7 \pm 13.9\%\ min^{-1}$). These data indicated that the Ca^{2+} efflux via the forward mode of NCX_{mito} is dependent on $\Delta\Psi_{mito}$. However, the Ca^{2+} efflux might be saturated at negative $\Delta\Psi_{mito}$ when Ca^{2+}_{mito} concentration is lower.

Ca^{2+} influx through the reverse mode of NCX_{mito}

The voltage dependence of the reverse mode of NCX_{mito} was studied in Fig. 6. In this series of experiments, 7 μM ruthenium red, 0.1 μM cyclosporin A and 10 μM SM20550 ($IC_{50} = 10$ nM; Yamamoto *et al.* 2000) were added to the bath solution to suppress the mitochondrial Ca^{2+} uniporter, PTP, and the mitochondrial Na^+–H^+ exchange, respectively. Applying 600 nM Ca^{2+}_c did not significantly increase the Rhod-2 fluorescence, but membrane depolarization by 1 μM FCCP and 2 μM oligomycin (FCCP + Olig, Fig. 6*A*) remarkably augmented the Rhod-2 fluorescence ($Na^+_c = 20$ mM). Essentially the same result was obtained with 1 μM FCCP alone (Fig. 7*A*), or 10 μM antimycin A and 2 μM oligomycin (Anti + Olig, Fig. 7*B*). CGP-37157 (30 μM) did not significantly affect the Rhod-2 fluorescence with 600 nM Ca^{2+}_c at the intact Ψ_{mito}, but greatly attenuated the depolarization-induced Ca^{2+}_{mito} rise (data not shown), indicating that the Ca^{2+}_{mito} increase is mediated via the reverse mode of NCX_{mito}. Although FCCP might induce mitochondrial ATP depletion via the reverse of F_0/F_1-ATPase (Nicholls & Budd, 2000) and Ca^{2+} release from sarcoplasmic reticulum (Landolfi *et al.* 1998), these effects were not involved in the Ca^{2+}_{mito} increase because no significant difference was found both in the maximum increase of Ca^{2+}_{mito} (Fig. 6*B*) and the change of $\Delta\Psi_{mito}$ (Table 1) among the procedures with FCCP, FCCP + Olig, and Anti + Olig. However, lesser $\Delta\Psi_{mito}$ depolarization by NS1619 or NS1619 + Sub(−) tended to induce a lower increase in Ca^{2+}_{mito}. This suggested a strong voltage dependence of the reverse mode of NCX_{mito}. To further confirm the voltage-dependent nature of the reverse mode of NCX_{mito}, we measured the change in $\Delta\Psi_{mito}$ with TMRE upon inducing the reverse mode of NCX_{mito} (Fig. 6*C*). Applying 600 nM Ca^{2+} to the myocyte that was treated with the NS1619 + Sub(−) procedure increased the TMRE fluorescence twofold (triangles), indicating membrane hyperpolarization. A larger increase in the TMRE fluorescence was induced in myocytes treated with Anti + Olig (open circles) probably because of larger

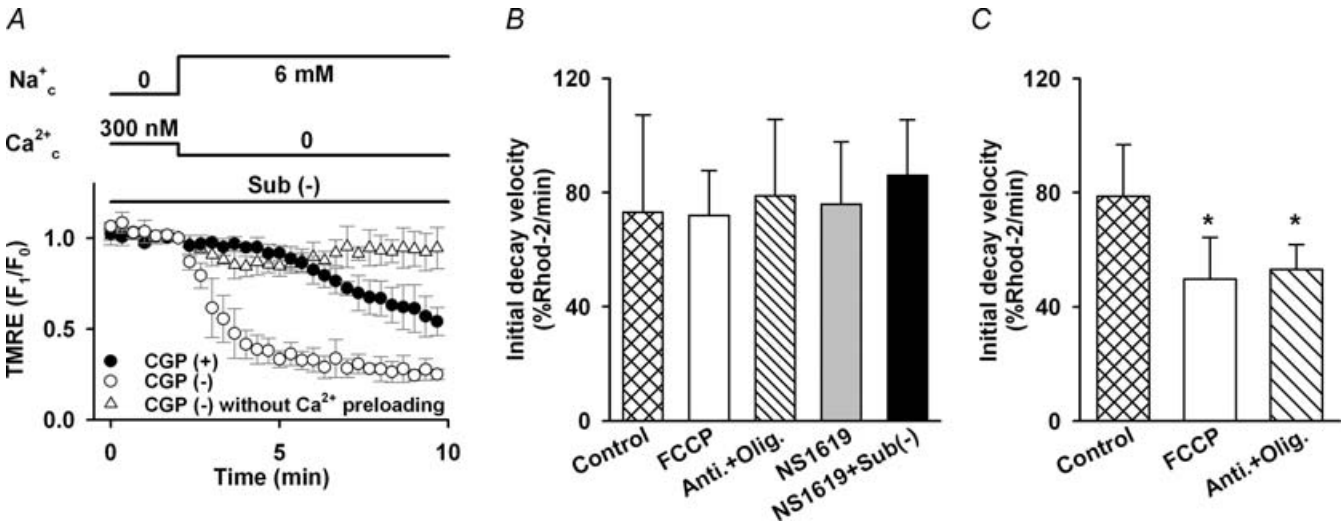

Figure 5. Voltage dependence of forward mode of NCX_{mito}
A, $\Delta\Psi_{mito}$ change upon activation of forward mode of NCX_{mito} with (●, $n = 4$) and without (○, $n = 6$) 30 μM CGP-37157. TMRE fluorescence was normalized to the one before changing the bath solution to that containing 6 mM Na^+ and no Ca^{2+}. Mitochondria were preloaded with Ca^{2+} for 10 min with the protocol in Fig. 4. Without Ca^{2+} preloading, no remarkable change in TMRE fluorescence was induced (△, $n = 5$). *B*, $\Delta\Psi_{mito}$ dependence of forward mode of NCX_{mito} in intact (Control) and depolarized mitochondria preloaded with 300 nM Ca^{2+}_c. The initial decay velocity of Rhod-2 fluorescence was measured at control and depolarized $\Delta\Psi_{mito}$ by 1 μM FCCP, 10 μM antimycin A and 2 μM oligomycin (Anti + Olig), 10 μM NS1619, and 10 μM NS1619 without mitochondrial substrates (NS1619 + Sub(−)). The initial decay velocity was not significantly different among the five groups. $n = 5$–24. *C*, $\Delta\Psi_{mito}$ dependence of forward mode of NCX_{mito} in mitochondria preloaded with 800 nM Ca^{2+}_c. The initial decay velocity was measured at control and depolarized $\Delta\Psi_{mito}$ by FCCP or Anti + Olig. The initial decay velocity of FCCP or Anti + Olig was significantly smaller than the control group (*$P < 0.05$). $n = 7$–11. In these experiments, 0.1 μM cyclosporin A was added to inhibit PTP.

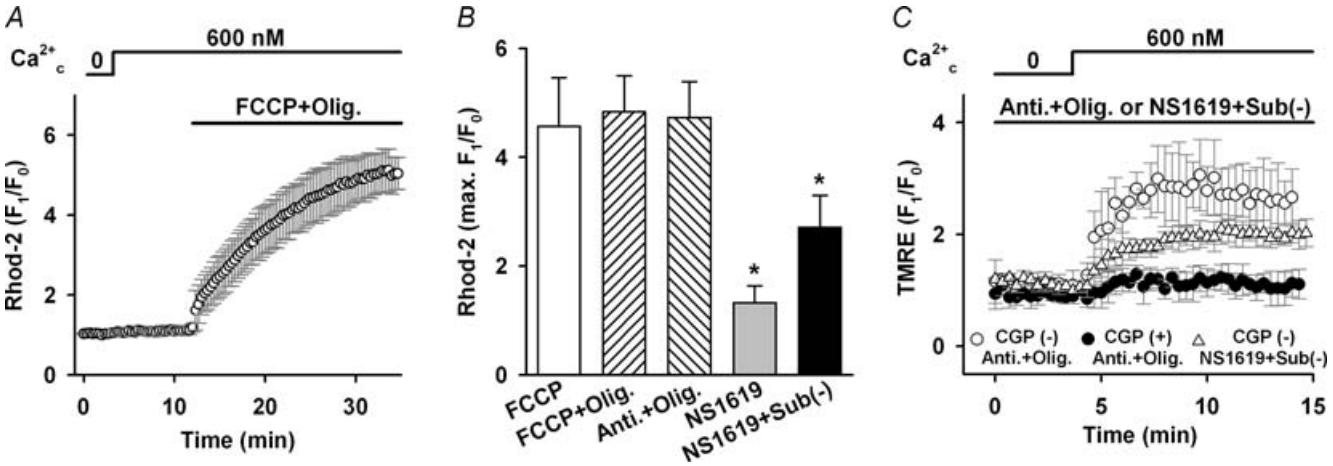

Figure 6. Voltage dependence of reverse mode of NCX_{mito}
A, the increase in Ca^{2+}_{mito} change upon $\Delta\Psi_{mito}$ depolarization. Ca^{2+} (600 nM) was added as denoted at the top of graph under the conditions that Ca^{2+} uniporter and PTP were suppressed. Na^+_c concentration was 20 mM. Depolarization by 1 μM FCCP and 2 μM oligomycin (FCCP + Olig) significantly augmented the Rhod-2 fluorescence. *B*, summary of Ca^{2+}_{mito} increase induced by five depolarization procedures. The maximum increases of Rhod-2 florescence were 4.6 ± 0.9, 4.8 ± 0.7, 4.7 ± 0.7, 1.3 ± 0.3 and 2.7 ± 0.6 times, respectively, in the presence of FCCP, FCCP + Olig, Anti + Olig, NS1619, and NS1619 + Sub(−). $n = 5$–27. The maximum increase by NS1619 or NS1619 + Sub(−) was significantly small than the other groups ($^*P < 0.05$). *C*, $\Delta\Psi_{mito}$ change upon activation of reverse mode of NCX_{mito}. The myocytes loaded with TMRE were superfused with the bath solution containing Anti + Olig or NS1619 + Sub(−). The reverse mode of NCX_{mito} was induced by adding 600 nM Ca^{2+}_c with (●) and without (○ and △) CGP-37157. $n = 5$–10.

activity of NCX_{mito} (see Fig. 6*B*). CGP-37157 significantly inhibited the fluorescence increase (filled circles, Fig. 6*C*). These data indicated that NCX_{mito} is electrogenic also in the reverse mode. The direction of $\Delta\Psi_{mito}$ change was opposite to that induced by the forward mode of NCX_{mito} (Fig. 5*A*), and consistent with the notion that the Na^+ translocation step is electrogenic.

The Na^+_c dependence of the reverse mode of NCX_{mito} was studied in Fig. 7. Although the reverse mode of NCX_{mito} was expected to be enhanced by removing Na^+_c, the Na^+_c removal almost completely abolished the depolarization-induced Ca^{2+}_{mito} increase by FCCP alone (Fig. 7*A*) or antimycin A and oligomycin (Anti + Olig, Fig. 7*B*). These results are consistent with data in Fig. 2,

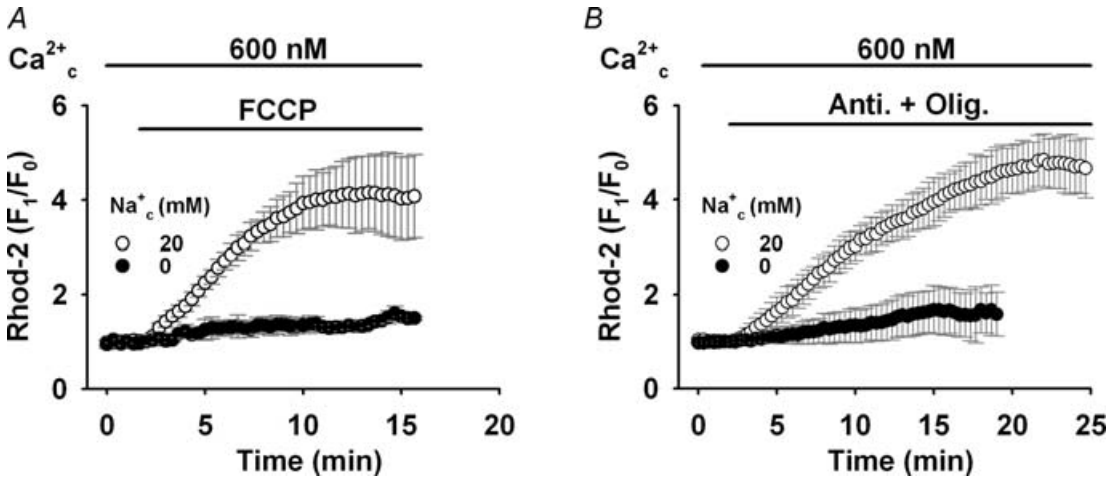

Figure 7. Effects of Na^+_c on depolarization-induced Ca^{2+}_{mito} increase by 1 μm FCCP (*A*) or 10 μm antimycin A and 2 μm oligomycin (*B*)
The protocol is the same as in Fig. 6*A*. Removal of Na^+_c significantly attenuated the depolarization-induced Ca^{2+}_{mito} increase. Data are with 20 mM Na^+_c (○: $n = 7$, *A*; $n = 7$, *B*) and without Na^+_c (●: $n = 5$, *A*; $n = 6$, *B*).

but apparently conflict with the general characteristics of plasma membrane NCX.

The above experimental findings strongly indicated that the Na_c^+-dependent Ca^{2+}_{mito} *decrease* at intact $\Delta\Psi_{mito}$ and *increase* at depolarized $\Delta\Psi_{mito}$ are mediated via voltage-dependent and electrogenic NCX_{mito}. We further studied dependences of NCX_{mito} on Na_c^+ and $\Delta\Psi_{mito}$ by computer simulations.

Simulation study on NCX_{mito}

As described in the Appendix, our computer model of NCX_{mito} assumed the following hypotheses: (i) electrogenic $3Na^+/1Ca^{2+}$ exchange, (ii) the carrier-bound $3Na^+$ has one positive charge, and (iii) a consecutive exchange which consists of two states of the carrier (E_1 and E_2). We examined how this model can explain our and previous experimental data. In Fig. 8*A*, the voltage dependence of Ca^{2+} efflux was simulated at various Ca^{2+}_{mito}; 300 nM (black dashed line), 1000 nM (grey line) and 3000 nM (green line). The saturation of the Ca^{2+} efflux with 300 nM Ca^{2+}_{mito} at negative $\Delta\Psi_{mito}$ is in agreement with the result in Fig. 5*B*. However, increasing Ca^{2+}_{mito} steepened the voltage dependence. The steep $\Delta\Psi_{mito}$ dependence at higher Ca^{2+}_{mito} concentrations is in agreement with the present (Fig. 5*C*) and previous experiment by Crompton *et al.* (1977) demonstrating that depolarization by an uncoupler attenuated the Na_c^+-dependent Ca^{2+} efflux from isolated mitochondria pre-loaded with 1000–3000 nM Ca_c^{2+}. The voltage dependence of the reverse mode of NCX_{mito} was simulated under the experimental conditions of Fig. 6 (Fig. 8*B*). We assumed a linear relationship between Na_c^+ and Na^+ in the mitochondrial matrix (Na^+_{mito}) according to experimental data by Jung *et al.* (1992) as described in the Appendix; $Na_c^+/Na^+_{mito} = 8.6$ at intact $\Delta\Psi_{mito}$ (red line in Fig. 8*B*) and $Na_c^+/Na^+_{mito} = 2.2$ at depolarized $\Delta\Psi_{mito}$ (blue line in Fig. 8*B*). It was predicted that the Ca^{2+} influx is negligible at intact $\Delta\Psi_{mito}$ (−180 to about −150 mV), but the $\Delta\Psi_{mito}$ depolarization and the following increase in Na^+_{mito}

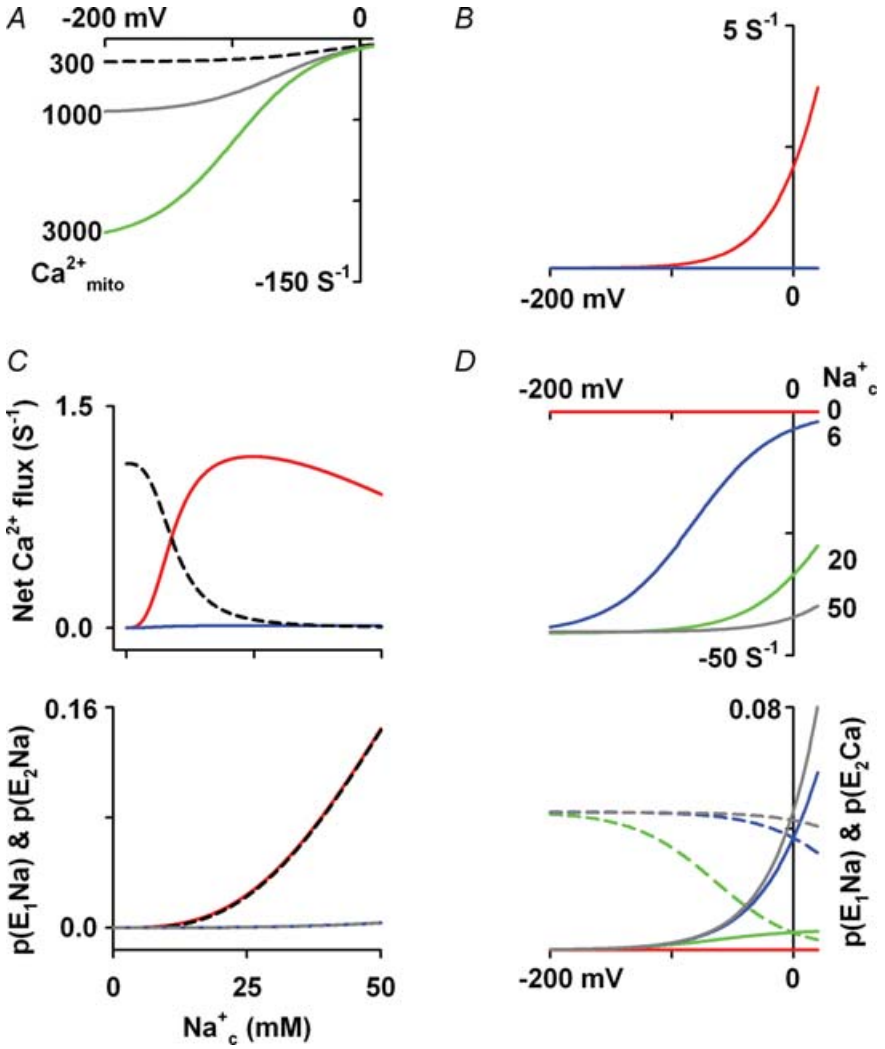

Figure 8. Simulation of net Ca^{2+} flux via NCX_{mito}
A, relation between net Ca^{2+} flux and $\Delta\Psi_{mito}$ of forward mode of NCX_{mito}. $Ca^{2+}_{mito} = 300$, 1000 and 3000 nM as denoted at the left of graph. $Na_c^+ = 6$ mM, $Ca_c^{2+} = 0$ and $Na^+_{mito} = Na_c^+/8.6$ mM. *B*, relation between net Ca^{2+} flux and $\Delta\Psi_{mito}$ of reverse mode of NCX_{mito}. $Na_c^+ = 20$ mM, $Ca_c^{2+} = 600$ nM, $Ca^{2+}_{mito} = 0$, and with $Na^+_{mito} = Na_c^+/2.2$ (red line) or $Na_c^+/8.6$ mM (blue line). *C*, Na_c^+ dependence of Ca^{2+} influx via reverse mode (upper panel), and $P(E_2Na)$ and $P(E_1Na)$ (at lower panel). $Ca^{2+}_{mito} = 0$, $Ca_c^{2+} = 300$ nM and $\Delta\Psi_{mito} = 0$ mV. At upper panel, Na^+_{mito} was set to a fixed value (4 mM, black dashed line), $Na_c^+/8.6$ (blue line), and $Na_c^+/2.2$ mM (red line), respectively. In lower panel, $P(E_2Na)$ and $P(E_1Na)$ were plotted setting $Na^+_{mito} = Na_c^+/8.6$ (blue line and grey dashed line, respctively) and $Na^+_{mito} = Na_c^+/2.2$ mM (red and black dashed line, respectively). *D*, effects of Na_c^+ on Ca^{2+} efflux via forward mode of NCX_{mito}. Upper and lower panels represent the net Ca^{2+} flux–$\Delta\Psi$ relationship and the $\Delta\Psi$ dependence of $P(E_1Na)$ (continuous lines) and $P(E_2Ca)$ (dashed lines). $Na^+_{mito} = Na_c^+/8.6$ mM, $Ca^{2+}_{mito} = 1000$ nM, and $Ca_c^{2+} = 0$. Na_c^+ is denoted at right of graph.

permeability strongly augment the Ca^{2+} influx at $\Delta\Psi_{mito}$ more than −100 mV (red line in Fig. 8*B*). These results are comparable to the experimental result in Fig. 6*A*. The Na^+_c dependence of the reverse model of NCX_{mito} at depolarized $\Delta\Psi_{mito}$ was studied in Fig. 8*C*. Increasing Na^+_c monotonically attenuated the Ca^{2+} influx when a constant Na^+_{mito} (4 mM) was assumed (black dashed line in upper panel of Fig. 8*C*) because of the competitive inhibition of the Ca^{2+}_c binding by Na^+_c. If the ratio of Na^+_c/Na^+_{mito} under the normal condition (8.6) was assumed, no significant increase in the Ca^{2+} influx was evoked (blue line in the upper panel of Fig. 8*C*). This is because the probability of carriers bound with Na^+_c and Na^+_{mito} ($P(E_1Na)$ and $P(E_2Na)$, respectively) did not significantly increase (grey dashed line and blue line in lower panel of Fig. 8*C*). However, if the ratio under the depolarized condition (2.2) was assumed, $P(E_1Na)$ and $P(E_2Na)$ remarkably increased as increasing Na^+_c (black dashed line and red line in the lower panel of Fig. 8*C*), and the Ca^{2+} influx augmented as increasing Na^+_c and peaked approximately at 20 mM Na^+_c (red line in upper panel of *C*). This relation is consistent with the experimental finding in Fig. 2*D*.

The above simulation results demonstrated that the voltage-dependent nature of NCX_{mito} plays key roles in regulating Ca^{2+}_{mito} concentration, and predicted that the increase in mitochondrial Na^+ permeability at depolarized $\Delta\Psi_{mito}$ contributes to the apparently opposite Na^+_c dependence of the reverse mode of NCX_{mito}.

Discussion

The voltage dependence or electrogenicity of NCX_{mito} has been controversial since NCX_{mito} was first discovered by Carafoli *et al.* (1974). In the present study, we for the first time recorded the $\Delta\Psi_{mito}$ change upon inducing the forward and reverse mode of NCX_{mito}. This finding strongly indicated that NCX_{mito} is electrogenic. The direction of $\Delta\Psi_{mito}$ change suggested that net positive charge moves in the direction of net Na^+ flux, or that net negative charge moves in the direction of net Ca^{2+} flux. The Na^+ translocation step of NCX_{mito} may be a major electrogenic step, analogously to the plasma membrane NCX (Hilgemann *et al.* 1991; Matsuoka & Hilgemann, 1992; Powell *et al.* 1993). The latter is also possible as shown in plasma membrane NCX (Niggli & Lederer, 1991). Affolter & Carafoli (1980) failed to observe the $\Delta\Psi_{mito}$ change upon inducing the Na^+_c-dependent Ca^{2+} efflux from isolated mitochondria. The $\Delta\Psi_{mito}$ change induced by NCX_{mito} might be easily compensated by H^+ pumping via the respiratory chain. This hypothesis was validated in the experiment of Fig. 5*A* where the expected change in $\Delta\Psi_{mito}$ was observed when the respiratory chain was inhibited.

The voltage dependence of NCX_{mito} may depend on ionic conditions. The Na^+_c-dependent Ca^{2+} efflux from mitochondria preloaded with a relatively low concentration of Ca^{2+}_c (300 nM) was not significantly affected by $\Delta\Psi_{mito}$ depolarization (Fig. 5*B*), but it was indeed affected when preloaded with higher Ca^{2+}_c (800 nM, Fig. 5*C*). The latter finding was consistent with the data of Crompton *et al.* (1977) demonstrating that $\Delta\Psi_{mito}$ depolarization by an uncoupler greatly attenuated the Na^+_c-dependent Ca^{2+} efflux from isolated mitochondria preloaded with 1000–3000 nM Ca^{2+}_c. Our computer simulation predicted that the slope of net Ca^{2+} flux of the forward mode of NCX_{mito} depends on Ca^{2+}_{mito} concentration (Fig. 8*A*) and supported the experimental findings. Our computer model further predicted that the Na^+_c concentration also affects the slope of voltage dependence as shown in Fig. 8*D*. The increase in Na^+_c concentration augmented the probability of exchanger bound with Na^+_c ($P(E_1Na)$) and that with Ca^{2+}_{mito} ($P(E_2Ca)$) at higher $\Delta\Psi_{mito}$, resulting in the augmentation of Ca^{2+} efflux at higher $\Delta\Psi_{mito}$ and the attenuation of the voltage dependence. On the other hand, a substantial increase in the Ca^{2+} influx via the reverse mode of NCX_{mito} was induced by the $\Delta\Psi_{mito}$ depolarization (Fig. 6*A*). This marked effect of depolarization is probably due to the steep voltage dependence of NCX_{mito} under the experimental conditions (20 mM Na^+_c, Fig. 8*B*). Details of the voltage dependence of NCX_{mito} remain to be clarified by direct measurement of NCX_{mito}-associated current.

Saotome *et al.* (2005) suggested that $\Delta\Psi_{mito}$ dissipation does not remarkably affect Ca^{2+} efflux via NCX_{mito} when preloaded with 300 nM Ca^{2+}_c. Their findings might be in line with our conclusion. However, in their experiments, about a half of the Ca^{2+} efflux was mediated via non-NCX_{mito} mechanism(s) which was insensitive to Na^+_c and diltiazem (an inhibitor of NCX_{mito}), and the speed of the Ca^{2+} efflux was slower. Experimental temperature (22 *versus* 37°C) might affect the turnover rate of NCX_{mito}.

As demonstrated in the current and previous studies (Sedova & Blatter, 2000; Malli *et al.* 2003), Na^+_c significantly affects Ca^{2+}_{mito} concentration through the forward mode of NCX_{mito}. However, a variety of $K_{1/2}$ values of NCX_{mito} for Na^+_c has been reported in cardiac myocytes and other cells, ranging from 1 to 12 mM (Crompton *et al.* 1976, 1978; Coll *et al.* 1982; Fry *et al.* 1984; Wingrove & Gunter, 1986; Sedova & Blatter, 2000; Saotome *et al.* 2005; Fig. 4*B* from our data). Our computer simulation predicted that the affinity for Na^+_c is decreased by the $\Delta\Psi_{mito}$ depolarization, the increase in Ca^{2+}_{mito} or increase in Ca^{2+}_c concentration (data not shown). Thus the variability of the $K_{1/2}$ value is probably, at least in part, caused by the experimental conditions employed.

The most puzzling finding was the Na^+_c dependence of the reverse mode of NCX_{mito}. The dependence

was opposite to the general characteristics of plasma membrane NCX and the NCX_{mito} model (the black dashed line of the upper panel in Fig. 8*C*). However, the NCX_{mito} model well reproduced the experimentally obtained Na_c^+ dependence by adopting the relationship between Na_c^+ and Na_{mito}^+ in isolated mitochondria (Jung *et al.* 1992). Griffiths (1999) found that metabolic inhibition induced the collapse of $\Delta\Psi_{mito}$ and the Ca_{mito}^{2+} increase in rat cardiomyocytes and the Ca_{mito}^{2+} increase was attenuated by CGP-37157. Similar results were obtained in metabolically inhibited renal epithelial cells of Madin–Darby canine kidney (MDCK) and concomitant increases in Na_c^+ and Na_{mito}^+ were observed (Smets *et al.* 2004; Baron *et al.* 2005). It is logically expected that the increase in Na_c^+ *attenuates* the reverse mode of NCX_{mito}. However, as demonstrated by the present experiments and computer simulation, the increase in Na_c^+ up to 50 mM still induced significant Ca^{2+} influx via NCX_{mito} when $\Delta\Psi_{mito}$ was depolarized because of a possible increase in the Na^+ permeability of the mitochondrial membrane.

Several pathways of mitochondrial Na^+ flux have been proposed; Na^+–H^+ exchange for Na^+ efflux, and NCX_{mito}, Na^+ channel and PTP for Na^+ influx (Bernardi, 1999). Monocarboxylic acid transporter (lactate or pyruvate – Na^+ cotransporter; Takeo & Tanonaka, 2004) and mitochondrial K_{ATP} channels (Bernardinelli *et al.* 2006) may be another route for Na^+ influx. Although mechanisms of the depolarization-induced increase in Na^+ permeability has not been clarified, it might be speculated that the depolarization procedures employed in this study increased mitochondrial H^+, which in turn attenuated H^+ gradient across the mitochondrial membrane and inhibited Na^+ efflux via Na^+–H^+ exchanger. In our preliminary experiments, no remarkable difference was observed in the depolarization-induced Ca_{mito}^{2+} increase with or without SM20550, an inhibitor of mitochondrial Na^+–H^+ exchange. This might indicate that the Na^+–H^+ exchanger was already suppressed when $\Delta\Psi_{mito}$ was depolarized.

In this study, we did not calibrate Rhod-2 fluorescence due to the difficulty of accurate calibration, and assumed a linear relationship between the Rhod-2 fluorescence and Ca_{mito}^{2+} concentration because the almost proportional relation to Ca_{mito}^{2+} concentration of Hela cells was reported in the range that the intensity greatly changes (Collins *et al.* 2001). Similarly, the absolute value of $\Delta\Psi_{mito}$ could not be obtained in this study. The values of $K_{1/2}$ and $\Delta\Psi_{mito}$ may be slightly different if accurate calibrations of Rhod-2 and TMRE signals are achieved, but our conclusion about the voltage-dependent and electrogenic property of NCX_{mito} will be still valid. Our computer model is the first one that can well reproduce a wide range of experimental data of cardiac NCX_{mito}, but has several limitations because of the lack of quantitative experimental data about NCX_{mito}, such as the current–voltage relationship, affinities for Na_{mito}^+ and Ca_{mito}^{2+}, and the stoichiometry. Further experimental studies are needed to refine the model.

In summary, the cardiac NCX_{mito} is voltage dependent and electrogenic. The voltage- and Na_c^+-dependent natures of NCX_{mito} dynamically modulate Ca_{mito}^{2+} concentration in the cardiac myocyte.

Appendix

A model of NCX_{mito}

A computer model of NCX_{mito} was constructed based on a general scheme proposed by Crompton *et al.* (1977) and a computer model of sarcolemmal $3Na^+$–$1Ca^{2+}$ exchange (Powell *et al.* 1993) (Fig. 9). E_1 and E_2 are states that an ion binding site faces, cytoplasm and mitochondrial matrix, respectively. Instantaneous binding of Na^+ and Ca^{2+} to the carrier was assumed and the probability of the ion-bound carrier in the E_1 and E_2 states was expressed as follows.

$$P(E_1Na) = 1/(1 + (1 + ([Ca^{2+}]_c / K_dCa_c))(K_dNa_c/[Na^+]_c)^3)$$

$$P(E_2Na) = 1/(1 + (1 + ([Ca^{2+}]_{mito} / K_dCa_{mito}))(K_dNa_{mito}/[Na^+]_{mito})^3)$$

$$P(E_1Ca) = 1/(1 + (1 + (1 + ([Na^+]_c / K_dNa_c)^3)(K_dCa_c/[Ca^{2+}]_c))$$

$$P(E_2Ca) = 1/(1 + (1 + (1 + ([Na^+]_{mito} / K_dNa_{mito})^3)(K_dCa_{mito}/[Ca^{2+}]_{mito}))$$

$$K_dNa_c = 38\,mM,\ K_dCa_c = 0.0125\,mM,\ K_dNa_{mito} = 32\,mM,\ K_dCa_{mito} = 0.021\,mM$$

The Na^+-bound carrier was assumed to have one positive charge and rate constants (k_1–k_4) were expressed as follows.

$$k_1 = 1000\exp((\gamma - 1)F\Delta\psi_{mito}/R/T)(s^{-1}),\ \gamma = 0.2$$

$$k_2 = 1000\exp(\gamma F\Delta\psi_{mito}/R/T)(s^{-1})$$

$$k_3 = 1000(s^{-1})$$

$$k_4 = 1000(s^{-1})$$

where F is Faraday's constant (96.4867 C mmol^{-1}), R is the gas constant (8.3143 C mV K^{-1} mmol^{-1}), and T is absolute temperature (310 K).

Steady state probability that the exchanger locates in E_1 and E_2 state $P(E_1\text{total})$ and $P(E_2\text{total})$ and net Ca^{2+} flux

were calculated as below.

$$P(\mathrm{E_1total}) = \alpha/(\alpha+\beta), P(\mathrm{E_2total}) = 1 - P(\mathrm{E_1total})$$

$$\alpha = k_2 P(\mathrm{E_2Na}) + k_4 P(\mathrm{E_2Ca})$$

$$\beta = k_1 P(\mathrm{E_1Na}) + k_3 P(\mathrm{E_1Ca})$$

$$\mathrm{NetCa^{2+}flux} = -P(\mathrm{E_2total}) \bullet P(\mathrm{E_2Ca})\mathrm{k_4} + P(\mathrm{E_1total}) \bullet P(\mathrm{E_1Ca})k_3$$

Reversal potential of the NCX_{mito} current, which can be calculated with the Na^+ flux rate, should be the same as the equilibrium potential of $3Na^+$–$1Ca^{2+}$ exchange ($E_{Na/Ca}$).

$$E_{Na/Ca} = 3E_{Na} - 2E_{Ca}$$

This assumption yields a following constraint

$$\left(K_d Na_c^3 K_d Ca_{mito}\right)/\left(K_d Na_{mito}^3 K_d Ca_c\right) = 1$$

The values of the dissociation constant were determined so as to fit experimental data and this constraint.

In the present experiments, Na^+_{mito} concentration might change when changing Na^+_c. Na^+_{mito} concentration was estimated by the linear relation between Na^+_c and Na^+_{mito}, which was obtained in isolated mitochondria by Jung *et al.* (1992); $Na^+_c/Na^+_{mito} = 8.6$ at intact $\Delta\Psi_{mito}$ (grey line in Fig. 9*B*) and $Na^+_c/Na^+_{mito} = 2.2$ at depolarized $\Delta\Psi_{mito}$ (black line in Fig. 9*B*).

Figure 9*C* and *D* demonstrates the Na^+_c dependence of the forward mode and the Ca^{2+}_c dependence of the reverse mode of NCX_{mito}, respectively. Dissociation constants for Na^+_c and Ca^{2+}_c were determined to fit experimental data in Fig. 4*B* and data of Ca^{2+} and Na^+ fluxes measurement from reconstructed beef heart NCX_{mito} by Paucek & Jabrek (2004). The Na^+_c dependence of Ca^{2+} efflux via forward mode NCX_{mito} is also in agreement with the data of Paucek & Jabůrek (2004) under their experimental conditions (0 mV, 10 μM Ca^{2+}_{mito}, 0 Na^+_{mito} and 0 Ca^{2+}_c).

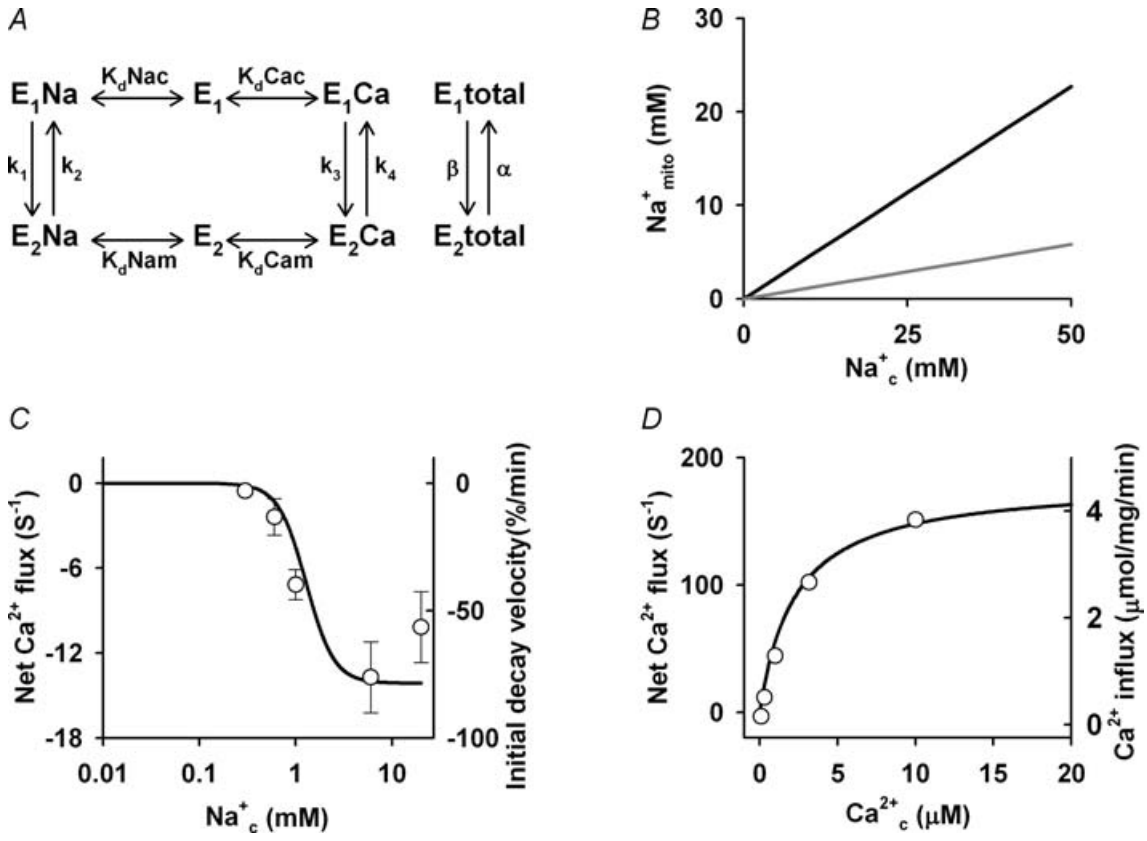

Figure 9. Dependence of NCX_{mito} model on Na^+_c and Ca^{2+}_c
A, a scheme of NCX_{mito} model. *B*, linear relations between Na^+_c and Na^+_{mito} at intact (grey) and depolarized (black) $\Delta\Psi_{mito}$ reproduced from Jung *et al.* (1992). *C*, Na^+_c dependence of Ca^{2+} efflux via forward mode of NCX_{mito}. The continous line is a model simulation ($Na^+_{mito} = Na^+_c/8.6$ mM, $Ca^{2+}_{mito} = 300$ nM, $Ca^{2+}_c = 0$ and $\Delta\Psi_{mito} = -180$ mV). Circles are experimental data from Fig. 4*B* in the present study. *D*, Ca^{2+}_c dependence of Ca^{2+} influx via reverse mode of NCX_{mito}. The continous line is a model simulation ($Na^+_{mito} = 25$ mM, $Na^+_c = 0$, $Ca^{2+}_{mito} = 0$ and $\Delta\Psi_{mito} = 0$ mV). Circles are experimental data by Paucek & Jabrek (2004).

References

Affolter H & Carafoli E (1980). The Ca^{2+}-Na^{+} antiporter of heart mitochondria operates electroneutrally. *Biochem Biophys Res Commun* **95**, 193–196.

Balaban RS (2002). Cardiac energy metabolism homeostasis: role of cytosolic calcium. *J Mol Cell Cardiol* **34**, 1259–1271.

Baron S, Caplanusi A, van de Ven M, Radu M, Despa S, Lambrichts I, Ameloot M, Steels P & Smets I (2005). Role of mitochondrial Na^{+} concentration, measured by CoroNa Red, in the protection of metabolically inhibited MDCK cells. *J Am Soc Nephrol* **16**, 3490–3497.

Bernardi P (1999). Mitochondrial transport of cations: channels, exchangers, and permeability transition. *Physiol Rev* **79**, 1127–1155.

Bernardinelli Y, Azarias G & Chatton JY (2006). In situ fluorescence imaging of glutamate-evoked mitochondrial Na^{+} responses in astrocytes. *Glia* **54**, 460–470.

Brand MD (1985). The stoichiometry of the exchange catalysed by the mitochondrial calcium/sodium antiporter. *Biochem J* **229**, 161–166.

Brookes PS, Yoon Y, Robotham JL, Anders MW & Sheu SS (2004). Calcium, ATP, and ROS: a mitochondrial love-hate triangle. *Am J Physiol Cell Physiol* **287**, C817–C833.

Carafoli E, Tiozzo R, Lugli G, Crovetti F & Kratzing C (1974). The release of calcium from heart mitochondria by sodium. *J Mol Cell Cardiol* **6**, 361–371.

Cherednichenko G, Zima AV, Feng W, Schaefer S, Blatter LA & Pessah IN (2004). NADH oxidase activity of rat cardiac sarcoplasmic reticulum regulates calcium-induced calcium release. *Circ Res* **94**, 478–486.

Coll KE, Joseph SK, Corkey BE & Williamson JR (1982). Determination of the matrix free Ca^{2+} concentration and kinetics of Ca^{2+} efflux in liver and heart mitochondria. *J Biol Chem* **257**, 8696–8704.

Collins TJ, Lipp P, Berridge MJ & Bootman MD (2001). Mitochondrial Ca^{2+} uptake depends on the spatial and temporal profile of cytosolic Ca^{2+} signals. *J Biol Chem* **276**, 26411–26420.

Cox DA, Conforti L, Sperelakis N & Matlib MA (1993). Selectivity of inhibition of Na^{+}-Ca^{2+} exchange of heart mitochondria by Benzothiazepine CGP-37157. *J Cardivasc Pharmacol* **21**, 595–599.

Crompton M, Capano M & Carafoli E (1976). The sodium-induced efflux of calcium from heart mitochondria. *Eur J Biochem* **69**, 453–462.

Crompton M, Knzi M & Carafoli E (1977). The calcium-induced and sodium-induced effluxes of calcium from heart mitochondria. *Eur J Biochem* **79**, 549–558.

Crompton M, Moser R, Rüdi H & Carafoli E (1978). The interrelations between the transport of sodium and calcium in mitochondria of various mammalian tissues. *Eur J Biochem* **82**, 25–31.

Fry CH, Powell T, Twist VW & Ward JPT (1984). The effects of sodium, hydrogen and magnesium ions on mitochondrial calcium sequestration in adult rat ventricular myocytes. *Proc R Soc Lond B Biol Sci* **223**, 239–254.

Griffiths EJ (1999). Reversal of mitochondrial Na/Ca exchange during metabolic inhibition in rat cardiomyocytes. *FEBS Lett* **453**, 400–404.

Gunter TE & Pfeiffer DR (1990). Mechanisms by which mitochondria transport calcium. *Am J Physiol Cell Physiol* **258**, C755–C786.

Hajnoczky G, Csordas G, Das S, Garcia-Perez C, Saotome M, Sinha Roy S & Yi M (2006). Mitochondrial calcium signaling and cell death: approaches for assessing the role of mitochondrial Ca^{2+} uptake in apoptosis. *Cell Calcium* **40**, 553–560.

Hilgemann DW, Nicoll DA & Philipson KD (1991). Charge movement during Na^{+} translocation by native and cloned cardiac Na^{+}/Ca^{2+} exchanger. *Nature* **352**, 715–718.

Jo H, Noma A & Matsuoka S (2006). Calcium-mediated coupling between mitochondrial substrate dehydrogenation and cardiac workload in single guinea-pig ventricular myocytes. *J Mol Cell Cardiol* **40**, 394–404.

Jung DW, Apel LM & Brierley GP (1992). Transmembrane gradients of free Na^{+} in isolated heart mitochondria estimated using a fluorescent probe. *Am J Physiol Cell Physiol* **262**, C1047–C1055.

Jung DW, Baysal K & Brierley GP (1995). The sodium-calcium antiport of heart mitochondria is not electroneutral. *J Biol Chem* **270**, 672–678.

Kirichok Y, Krapivinsky G & Clapham DE (2004). The mitochondrial calcium uniporter is a highly selective ion channel. *Nature* **427**, 360–364.

Landolfi B, Curci S, Debellis L, Pozzan T & Hofer AM (1998). Ca^{2+} homeostasis in the agonist-sensitive internal store: functional interactions between mitochondria and the ER measured in situ in intact cells. *J Cell Biol* **142**, 1235–1243.

Lin X, Jo H, Sakakibara Y, Tambara K, Kim B, Komeda M & Matsuoka S (2006). β-Adrenergic stimulation does not activate Na^{+}/Ca^{2+} exchange current in guinea pig, mouse, and rat ventricular myocytes. *Am J Physiol Cell Physiol* **290**, C601–C608.

McCormack JG, Halestrap AP & Denton RM (1990). Role of calcium ions in regulation of mammalian intramitochondrial metabolism. *Physiol Rev* **70**, 391–425.

McGuinness O, Yafel N, Costi A & Crompton M (1990). The presence of two classes of high-affinity cyclosporin A binding sites in mitochondria. *Eur J Biochem* **194**, 671–679.

Malli R, Frieden M, Osibow K, Zoratti C, Mayer M, Demaurex N & Graier WF (2003). Sustained Ca^{2+} transfer across mitochondria is essential for mitochondrial Ca^{2+} buffering, store-operated Ca^{2+} entry, and Ca^{2+} store refilling. *J Biol Chem* **278**, 44769–44779.

Matsuoka S & Hilgemann DW (1992). Steady-state and dynamic properties of cardiac sodium-calcium exchange. Ion and voltage dependencies of the transport cycle. *J Gen Physiol* **100**, 963–1001.

Matsuoka S, Jo H, Sarai N & Noma A (2004). An in silico study of energy metabolism in cardiac excitation-contraction coupling. *Jpn J Physiol* **54**, 517–522.

Nicholls DG & Budd SL (2000). Mitochondra and neuronal survival. *Physiol Rev* **80**, 315–360.

Niggli E & Lederer WJ (1991). Molecular operations of the sodium-calcium exchanger revealed by conformation currents. *Nature* **349**, 621–624.

O'Reilly CM, Fogarty KE, Drummond RM, Tuft RA & Walsh JV Jr (2003). Quantitative analysis of spontaneous mitochondrial depolarizations. *Biophys J* **85**, 3350–3357.

O'Rourke B (2007). Mitochondrial ion channels. *Annu Rev Physiol* **69**, 19–49.

Patton C, Thompson S & Epel D (2004). Some precautions in using chelators to buffer metals in biological solutions. *Cell Calcium* **35**, 427–431.

Paucek P & Jabrek M (2004). Kinetics and ion specificity of Na^+/Ca^{2+} exchange mediated by the reconstituted beef heart mitochondrial Na^+/Ca^{2+} antiporter. *Biochim Biophys Acta* **1659**, 83–91.

Pierce GN & Czubryt MP (1995). The contribution of ionic imbalance to ischemia/reperfusion-induced injury. *J Mol Cell Cardiol* **27**, 53–63.

Piper HM, Meuter K & Schafer C (2003). Cellular mechanisms of ischemia-reperfusion injury. *Ann Thorac Surg* **75**, S644–S648.

Powell T, Noma A, Shioya T & Kozlowski RZ (1993). Turnover rate of the cardiac Na^+-Ca^{2+} exchanger in guinea-pig ventricular myocytes. *J Physiol* **472**, 45–53.

Rottenberg H & Scarpa A (1974). Calcium uptake and membrane potential in mitochondria. *Biochemistry* **13**, 4811–4817.

Saotome M, Katoh H, Satoh H, Nagasaka S, Yoshihara S, Terada H & Hayashi H (2005). Mitochondrial membrane potential modulates regulation of mitochondrial Ca^{2+} in rat ventricular myocytes. *Am J Physiol Heart Circ Physiol* **288**, H1820–H1828.

Sato T, Saito T, Saegusa N & Nakaya H (2005). Mitochondrial Ca^{2+}-activated K^+ channels in cardiac myocytes: a mechanism of the cardioprotective effect and modulation by protein kinase A. *Circulation* **111**, 198–203.

Sedova M & Blatter LA (2000). Intracellular sodium modulates mitochondrial calcium signaling in vascular endothelial cells. *J Biol Chem* **275**, 35402–35407.

Shioya T (2007). A simple technique for isolating healthy heart cells from mouse models. *J Physiol Sci* **57**, 327–335.

Smets I, Caplanusi A, Despa S, Molnar Z, Radu M, Vandeven M, Ameloot M & Steels P (2004). Ca^{2+} uptake in mitochondria occurs via the reverse action of the Na^+/Ca^{2+} exchanger in metabolically inhibited MDCK cells. *Am J Physiol Renal Physiol* **286**, F784–F794.

Takeo S & Tanonaka K (2004). Na^+ overload-induced mitochondrial damage in the ischemic heart. *Can J Physiol Phamacol* **82**, 1033–1043.

Territo PR, Mootha VK, French SA & Balaban RS (2000). Ca^{2+} activation of heart mitochondrial oxidative phosphorylation: role of the F_0/F_1-ATPase. *Am J Physiol Cell Physiol* **278**, C423–C435.

Trolinger DR, Cascio WE & Lemasters JJ (1997). Selective loading of Rhod-2 into mitochondria shows mitochondrial Ca^{2+} transients during the contractile cycle in adult rabbit cardiac myocytes. *Biochem Biophys Res Commun* **236**, 738–742.

Van Dyke RW, Steer CJ & Scharschmidt BF (1984). Clathrin-coated vesicles from rat liver: Enzymatic profile and characterization of ATP-dependent proton transport. *Proc Natl Acad Sci U S A* **81**, 3108–3112.

Weiss JN, Korge P, Honda HM & Ping P (2003). Role of the mitochondrial permeability transition in myocardial disease. *Circ Res* **93**, 292–301.

Wingrove DE & Gunter TE (1986). Kinetics of mitochondrial calcium transport. II. A kinetic description of the sodium-dependent calcium efflux mechanism of liver mitochondria and inhibition by ruthenium red and by tetraphenylphosphonium. *J Biol Chem* **261**, 15166–15171.

Yamamoto S, Matsui K, Kitano M & Ohashi N (2000). SM-20550, a new Na^+/H^+ exchange inhibitor and its cardioprotective effect in ischemic/reperfused isolated rat hearts by preventing Ca^{2+}-overload. *J Cardiovasc Pharmacol* **35**, 855–862.

Acknowledgements

We are grateful to Professor Akinori Noma for his valuable support and advice. This study was supported by the Leading Project for Biosimulation and a Grant-in-Aid for Scientific Research from the Ministry of Education, Culture, Sports, Science and Technology of Japan (to S.M.) and COE Formation project for Genomic Analysis of Disease Model Animals with Multiple Genetic Alterations (to B.K.).